ELSEVIER

Measurements of heat transfer in a separated and reattaching flow with spatially varying thermal boundary conditions

J. M. Hacker and J. K. Eaton
Department of Mechanical Engineering, Stanford University, Stanford, CA

The effect of highly varying thermal boundary conditions on the convective heat transfer in a backward-facing step flow was investigated in a two-dimensional (2D) boundary-layer tunnel in air. A modified form of the transient heat transfer technique was used that allowed variable surface temperature distributions to be imposed by heating the test surface with a radiative lamp prior to cooling. The experiments were restricted to axial variations in surface temperature. Surface temperatures were measured with both cement-on foil thermocouples and thermochromic liquid crystal thermography. A semianalytic superposition technique was developed that was capable of predicting the heat transfer for any arbitrary axial surface temperature distribution, given the general solution or "Green's" function. The Green's function was measured to a limited spatial resolution by solving a simultaneous set of equations using data from 30 experiments. The techniques were developed and tested in a 2-D flat-plate boundary layer with $Re_{\delta 2}$ of 3500 at the leading edge and qualified against a well-verified boundary-layer code. The Green's function and inverse Green's function were then measured in a turbulent backward-facing step flow with Re based on step height of 26,000. In the separated flow, it was found that the effect of localized heating extended only a short distance upstream and downstream, and that the heat transfer was less sensitive to temperature boundary conditions than would be expected from attached flow behavior. This corroborates the conclusion of previous workers that the primary resistance to the heat transfer is localized near the wall. This localized behavior, and the spatial insensitivity of the Green's function, suggest that with proper scaling, the results could be extended to other separated flows.

Keywords: separated flow; Green's function; heat transfer; thermochromic liquid crystals

Introduction

In a general convective flow situation, the local rate of heat transfer to or from the wall is determined both by the global flow field or *fluid boundary conditions* and the global wall temperature distribution or *thermal boundary conditions*. The effect of the fluid boundary conditions on the heat transfer has been investigated in a large variety of flows for simple thermal boundary conditions. However, the effect of the thermal boundary conditions has only been studied in a few simple flows, primarily because of the lack of appropriate experimental techniques.

The effect of the thermal boundary conditions is an important consideration in any practical application in which the wall temperature varies significantly in the flow direction. For example, in a dump combustor, the location of a stationary flame, combined with a particular distribution of cooling passages in the wall, might lead to strong variations in the wall temperature. Similarly, in a heat exchanger, the periodic arrangement of the tubes and fins would produce strong wall temperature variations. In these situations, the actual heat transfer coefficient distribution can be expected to differ significantly from that predicted by available correlations.

The effect of thermal boundary conditions is also important when attempting to create a numerical heat transfer prediction model. There has been intense effort in developing turbulence models to predict the heat transfer in separated flows accurately, but most of the effort has focused on replicating a few datasets generated with simple thermal boundary conditions. Tuning heat transfer models to data with a narrow range of thermal boundary conditions will probably result in poor predictions when substantial variations in the wall temperature occur. Prior knowledge of the effect of the wall temperature distribution would help in synthesizing more realistic heat transfer models.

Most previous analytical and experimental studies are relevant only to simple global boundary conditions, such as constant

Address reprint requests to Dr. J. K. Eaton, Department of Mechanical Engineering, Stanford University, Stanford, CA 94305-3030, USA.

Received 10 March 1996; accepted 15 October 1996

Int. J. Heat and Fluid Flow 18: 131–141, 1997

655 Avenue of the Americas, New York, NY 10010

0142-727X/97/$17.00
PII S0142-727X(96)00142-9

wall heat flux or constant wall temperature. This is because only a few techniques exist that are capable of addressing complex thermal boundary conditions, and these are applicable only in simple situations. It is the goal of the present work to provide new information on the effect of variations in thermal boundary condition on separated and reattaching flow heat transfer. Before discussing the detailed objectives, we first review available treatments for varying thermal boundary conditions and the existing knowledge on separated flow heat transfer.

Existing techniques for varying thermal boundary conditions

Two-dimensional self-similar boundary layer. For two-dimensional (2-D), self-similar laminar and turbulent boundary layers, the heat transfer attributable to any arbitrary wall temperature distribution can be found by extending the "unheated starting length" solution via superposition. This method was pioneered by Tribus and Klein (1952) and is now described in many textbooks (Kays and Crawford 1993). Consider the 2-D Reynolds-averaged boundary-layer energy equation:

$$\bar{u}\frac{\partial \bar{T}}{\partial x}+\bar{v}\frac{\partial \bar{T}}{\partial y}-\frac{\partial}{\partial y}\left(\alpha\frac{\partial \bar{T}}{\partial y}-\overline{T'v'}\right)=0 \tag{1}$$

We restrict ourselves to small overall changes in the fluid temperature so that the fluid properties ρ, C_p, and μ are independent of temperature, and the energy equation is linear in temperature. The wall boundary conditions for the unheated starting length problem and a nondimensional unheated starting length solution θ are then defined:

$$T = T_\infty \quad \text{for} \quad x < \xi$$

$$T = T_0 \quad \text{for} \quad x \geq \xi$$

$$\theta(\xi, y, x) = \frac{T_0 - T(x,y)}{T_0 - T_\infty} \tag{2}$$

An arbitrary surface temperature distribution consisting of N discrete steps in surface temperature ΔT_{0i}, between which the temperature varies continuously with first derivative $\mathrm{d}T_0/\mathrm{d}x$ may be written as:

$$T_0(x) - T_\infty = \int_0^x \frac{\mathrm{d}T_0}{\mathrm{d}\xi}\,\mathrm{d}\xi + \sum_{i=1}^{N} T_{0i} \tag{3}$$

Given the step response described by Equation 2 and the linearity of the energy equation, the general flow-field temperature distribution is then,

$$T(x,y) - T_\infty = \int_0^x [1-\theta(\xi,x,y)]\frac{\mathrm{d}T_0}{\mathrm{d}\xi}\,\mathrm{d}\xi + \sum_{i=1}^{N}[1-\theta(\xi_i,x,y)]\,\Delta T_{0i} \tag{4}$$

and the wall heat flux may be calculated from Fourier's law,

$$q = -k\left.\frac{\partial T}{\partial y}\right|_{y=0} = k\left.\frac{\partial \theta}{\partial y}\right|_{\xi,x,0}(T_0 - T_\infty) \tag{5}$$

$$\left.\frac{\partial \theta}{\partial y}\right|_{\xi,x,0} = \frac{h(\xi,x)}{k} \tag{6}$$

Here $h(\xi, x)$ is the more usual form of the unheated starting length solution in terms of a heat transfer coefficient with units of W/m^2-K. Combining Equations 4–6, we have

$$q = \int_0^x h(\xi,x)\frac{\mathrm{d}T_0}{\mathrm{d}\xi}\,\mathrm{d}\xi + \sum_{i=1}^{N} h(\xi_i,x)\,\Delta T_{0i} \tag{7}$$

Given a particular unheated starting length solution, $h(\xi, x)$, Equation 7 predicts the wall heat transfer for any axial temperature distribution.

By applying Equation 7, we can show that the wall temperature distribution has a significant effect on the heat transfer coefficient distribution in a flat-plate, zero pressure gradient boundary layer. For example, in laminar flow, a linearly increasing wall temperature gives h everywhere about 61% higher than for a constant wall temperature; in turbulent flow, the increase is 13.4%. Similarly, in laminar flow, a constant heat flux boundary condition gives h everywhere 36% higher than a constant temperature boundary condition; in turbulent flow, the increase is 4%. Note that these differences are entirely due to differences in the thermal boundary conditions. If the wall temperature distribution is allowed to vary even more, there is virtually no limit on how high or low (even negative) the local heat transfer coefficient can be. In situations in which the surface temperature or heat flux varies sufficiently in the flow direction, the conventional heat transfer coefficient loses its utility altogether.

Electronics cooling channel flow. Anderson and Moffat (1992a, b) studied the flow between two closely spaced walls with a regular array of discrete heated components on one or both of the walls. They developed a technique specifically for this situation to account for the effect of the global thermal boundary conditions on the local heat transfer. Their method considers the surface as composed of a number of discrete elements, each of which is described by a single temperature and heat flux. Complete description of the heat transfer characteristics of the flow then requires knowledge of the effect of every element on every other element. Consider a two-dimensional (2-D) array of modules with row location n (the flow direction) and column location m (spanwise). The temperature at a single module may be represented by:

$$(T_{\text{element}} - T_{\text{in}})_{n,m} = \sum_{j=0}^{M}\sum_{i=0}^{n-1}\frac{q_{i,j}}{\dot{m}C_p}g_{n-i,m-j} \tag{8}$$

Here $\dot{m}$ is the mass flow rate of air through the channel, C_p is the specific heat of the flow, q_{ij} is the heat release at each element, and g_{ij} is the "two-dimensional discrete superposition kernel function" (Anderson's terminology)—a matrix similar to the heat transfer coefficient h. The kernel function g_{ij} can be measured directly by heating each individual element alternately and measuring the induced temperature at every other element.

Previous studies of separated flow heat transfer

Our interest is restricted to subsonic separated flows with simple geometry and Reynolds numbers sufficiently large that the flow is turbulent, at least downstream of separation. Reviews of the work prior to 1980 by Aung and Watkins (1979), Aung (1982) and Ota and Nishiyama (1987) present a consistent picture. An overall augmentation of the heat transfer coefficient is observed with a large peak believed to occur at the reattachment point. Ota and Nishiyama showed that the peak heat transfer coeffi-

cient can be well correlated by a function of the Prandtl number and a Reynolds number based on the reattachment length. However, Aung pointed out that "available information is limited to isolated ranges of the operating parameters ..." and that "quantitative predictions of the effects [of varying operating parameters] are not yet generally possible." All of the studies through 1980 used either constant temperature or constant heat flux wall boundary conditions with uniform free-stream temperature.

Two detailed studies were conducted by Vogel and Eaton (1984; 1985) for the planar backward facing step and by Baughn et al. (1984; 1989) for the axisymmetric sudden expansion. Vogel and Eaton measured spatially resolved heat transfer from a constant heat flux surface, and velocity and temperature profiles using laser anemometry and resistance thermometers. They concluded that the peak heat transfer rate occurs a short distance upstream of the mean reattachment point where turbulent intensities and length scales are maximum, and that the peak level is a strong function of the upstream boundary layer thickness. Baughn et al. measured the heat transfer downstream of a sudden pipe expansion for a range of Reynolds numbers and for both constant heat flux and constant temperature boundary conditions. For selected cases, they also measured mean temperature and velocity profiles. The change in boundary condition caused only minor changes in the Nusselt number distribution. Their measurements showed that the dominant resistance to heat transfer was concentrated very near the wall. Amano et al. (1983) performed both a numerical and experimental study of heat transfer in the axisymmetric sudden expansion. The spatial resolution of their measurements was too coarse to show the detail seen by Baughn et al., but the data did demonstrate the importance of the expansion ratio on the heat transfer coefficient.

A series of separated flow experiments in various tube geometries were conducted by Sparrow and coworkers using the naphthalene sublimination technique (Garcia and Sparrow 1987; Sparrow and Ohadi 1987; Sparrow 1988). Besides providing data for the various geometries, they also corroborated the conclusion that the peak in the heat transfer coefficient occurs upstream of the reattachment point. Mori et al. (1986) examined this conclusion in more detail by measuring the heat transfer coefficient in a planar backward-facing step and also measured the fluctuation of the reattachment location with a thermal tuft probe. They then inserted a guide plate in the free stream that dramatically reduced the unsteadiness of the reattachment region. They found a higher and narrower peak in the heat transfer coefficient with the peak closely aligned with the mean reattachment point. They concluded that the shift of the peak heat transfer upstream of the mean reattachment point had to do with the intermittent motions of the reattaching shear layer. Work by Shishov et al. (1988) has focused on the region of lower heat transfer coefficient in the fully separated zone upstream of reattachment. They concluded that "laminar boundary layer laws" were appropriate in the back-flow region. A similar conclusion was reached by Adams and Johnston (1988) using hydrodynamic data only.

In all of these experiments, the wall was only heated downstream of separation. An experiment by Orlov et al. (1984) used an apparatus in which only a small patch of the wall was heated. Their data were dramatically different from any previous experiment suggesting a strong sensitivity to the temperature boundary condition. An experiment by Wakisaka (1986) apparently heated all walls in the experimental apparatus, but the exact temperature boundary condition was difficult to determine from the paper. He showed a large temperature gradient across the separated shear layer in contrast to previous experiments. This again suggested a strong dependence of the results on the temperature boundary conditions. In a more well-controlled experiment, Chyu and Goldstein (1986) examined mass transfer in a rectangular cavity flow using naphthalene sublimination. Comparison to previous results suggested that the heat transfer coefficient was sensitive to the concentration boundary condition upstream of separation.

No previous studies systematically investigated the effect of varying wall temperature, but the studies that used nonstandard temperature boundary conditions had much different results suggesting a strong sensitivity. The present study shows that separated flow heat transfer is relatively insensitive to thermal boundary conditions. We now believe that we either misinterpreted Orlov et al. (1984) and Wakisaka (1986) or their results are erroneous.

Objectives

There were two objectives of this work. The first was to develop and verify an experimental technique capable of measuring heat transfer for arbitrary wall temperature distributions in separated flow situations. This technique was developed and verified in a conventional 2-D flat-plate boundary layer. The second objective was to use the new technique to make detailed measurement of the heat transfer in a backward-facing step flow and specifically to isolate the effect of the wall temperature distribution on the heat transfer. Only heating downstream of the backward facing step was considered.

Experimental apparatus and technique

The experiments were conducted in a 2-D horizontal wind tunnel used extensively for previous boundary-layer studies. The nominally steady-state tunnel was modified with a flap upstream of the working section to allow it to function in the transient mode. A version of the transient heat transfer technique was developed, which allows complex thermal boundary conditions to be imposed by heating a thin test surface to a specified temperature distribution prior to initiation of cooling.

Wind tunnel

Figure 1 is a schematic of the blower-driven, open-loop wind tunnel. Flow conditioning was provided by one honeycomb, four fine-mesh screens, a large pressure drop across the heat exchanger, and a 4:1 contraction. At the exit of the contraction, the boundary layers were tripped on all four walls. Although normally steady-state, the tunnel was modified with a flap upstream of the test section that could be used to divert flow into the

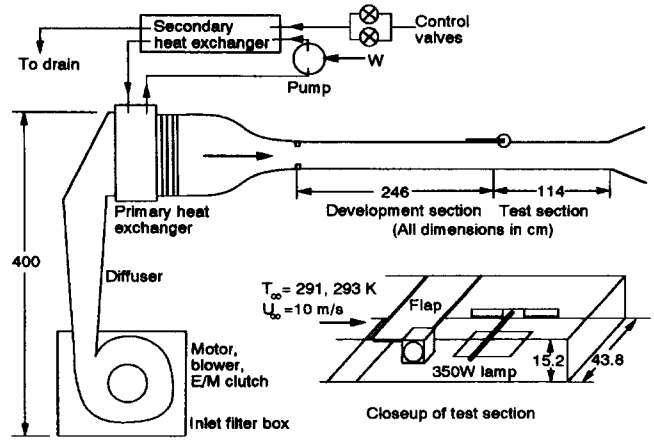

Figure 1 Transient wind tunnel with close-up of test section and diverter flap

room. The flap was controlled by a high-torque printed circuit board motor and could be opened in 0.3 seconds. This was essentially impulsive compared with the 15-s experiment duration. The tunnel velocity was measured 46 cm upstream of the test surface leading edge with a small Kiel probe, and the temperature was measured at the centerline, 38 cm downstream of the leading edge. The temperature control system made it possible to set the freestream temperature arbitrarily from 286–295 ± 0.1 K, yet maintain excellent spatial temperature uniformity (±0.05 K) throughout the flow.

Two basic flows were investigated: a conventional flat-plate boundary layer, and a backward-facing step flow. Figure 2 shows the geometry for both cases. (The backward-facing step assembly shown is removable.) In both cases, the velocity at the Kiel probe was set to 10.0 m/s, and the velocity profiles at x_1 and x_2 were measured with a hot wire. For the flat plate, the leading-edge velocity was 10.1 m/s, the momentum thickness was 5.3 mm, the momentum thickness Reynolds number was 3500, and the shape factor was 1.41. For the backward-facing step, the velocity at separation was 12.5 m/s, the momentum thickness was 2.4 mm, the momentum thickness Reynolds number was 1970, and the shape factor was 1.30.

The nonisothermal transient technique

Overview. The conventional transient heat transfer technique has been used widely since the 1950s for measurements in high-speed flows (see Schultz and Jones 1973), and more recently in low-speed flows (cf. Baughn et al. 1989). In the conventional method, the test surface is heated or the flow free-stream temperature is impulsively changed in order to establish an initial temperature difference between the model and the flow. At time = 0, the flow is impulsively initiated, and the temperature is monitored as the surface cools. By assuming a constant local heat transfer coefficient and mathematically modeling conduction within the substrate, we then calculate the heat transfer rate from the observed surface temperature history. The results are assumed to be representative of the constant wall temperature boundary condition, although the global surface temperature distribution is often allowed to change substantially over the course of the experiment.

The transient technique usually is applied in two distinct ways, each providing a particular simplification of the substrate conduction model used to calculate the heat transfer. In the "semi-infinite" version, the substrate thermal properties and dimensions are configured so that the heat penetration distance is small relative to the substrate thickness. Alternately, in the "thin-skin calorimeter" method, a two-layer surface is constructed: a low-diffusivity substrate covered by a thin sheet of conductive material. Experimental parameters are adjusted so that nearly all of the thermal energy transfer is to the thin skin, and a lumped heat capacity method is used to relate the heat transfer directly to the local rate of change of surface temperature. In both of these variations, transverse conduction caused by temperature gradients parallel to the surface generally is neglected.

For this work, the thin-skin calorimeter technique was modified to allow the specification of nearly arbitrary axial distributions of surface temperature. This was done in four steps. First, a thin, flat test surface was designed that acted as a "thermal capacitor" in the sense that a desired surface temperature distribution could be "painted" on relatively quickly with a radiative lamp and approximately maintained (within 20% or so) over the course of the experiment. Second, a long, thin heat lamp and motion control system were developed to do the heating. Third, a method was developed to calculate ahead of time how to move the lamp to create the desired surface temperature distribution. Fourth, a more sophisticated method of computing the heat flux from the measured transient temperatures was developed. In particular, it was necessary in some cases to account for axial diffusion within the substrate because of large second derivatives in the temperature profile.

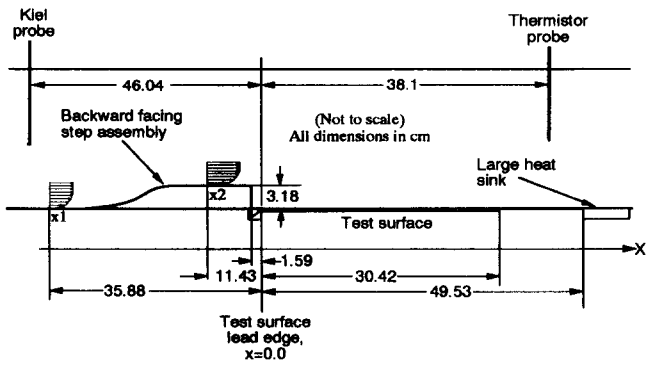

Figure 2 Flow geometry

Equipment. The test surface was a 3.52-mm (±13 μm) thick precision-ground plate of Pyrex 7740 glass. It measured 30.4 cm in the axial direction by 21.6 cm spanwise. The top surface was mounted flush with the tunnel floor, and the bottom was backed with 1.3 cm of balsa wood to nearly eliminate conduction. Before the leading edge, a small copper heat sink maintained a clean leading-edge temperature boundary condition. When inactive or warming up, the lamp was rested over a large copper heat sink 20 cm downstream of the test surface trailing edge. Fifteen fast response, copper/constantan (T-type) cement-on Omega surface thermocouples were attached along the test surface centerline. These thermocouples were 12.7-μm thick in the measurement region, well within the aerodynamically smooth limit for the flows tested. The entire surface was coated with Hallcrest BBG1 optically black paint and a thin layer of encapsulated thermochromic liquid crystals (Hallcrest BM/R65F10W/C17-10). The paint and liquid crystals together were approximately 55-μm thick. During each transient experiment, the thermocouples were monitored at 50 Hz by a standard A/D system, and the liquid crystal images were converted to temperature using Stanview 2.1—a dedicated TLC thermographic system developed at Stanford. A preliminary version of Stanview is described by Farina et al. (1994). The version used in this work is described in detail by Hacker and Eaton (1995). The thermocouples provided very high accuracy (±0.06 K) and low-noise measurements, but low spatial resolution (20 mm); the liquid crystals provided very high spatial resolution (0.5 mm), but lower accuracy (±0.50 K) and higher noise.

The radiative element was a 390 W cylindrical quartz resistive heater. The lamp was supported by an aluminum arm assembly that narrowed the effective aperture to 1 cm. The arm rode on a linear bearing, 1 mm above the test surface, and was driven by a dc stepper motor. The bearing assembly and motor were housed in a sealed box bolted to the left edge of the test section. The arm protruded through a thin slot in the tunnel wall, free to move along the working section. The dynamic response of the entire apparatus was such that accelerations up to 1 g and speeds up to 47 cm/s could be attained. Figure 3 shows the radiative heat flux distribution imposed on the test surface by the lamp as a function of radial distance from the lamp location. This heat flux profile was measured with the flow turned off by passing the lamp across the test plate at a steady velocity of 20 mm/s while monitoring the response of a single thermocouple near the center of the test surface. A finite-difference calculation of the

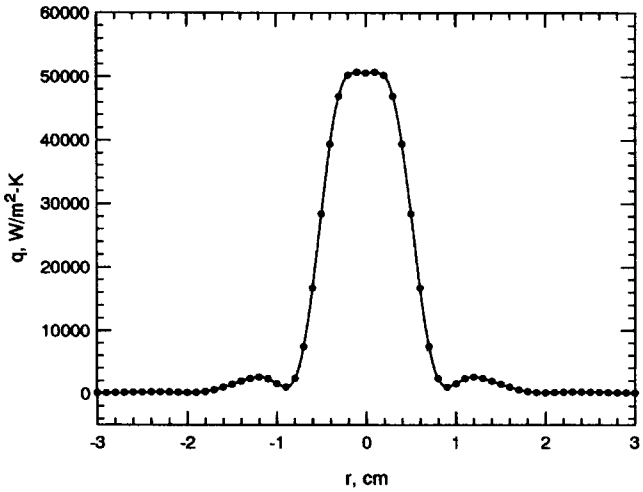

Figure 3 Lamp heat flux profile

transient heat conduction problem was then used to infer the heat flux distribution. Details of this calibration method are discussed in Hacker and Eaton (1995). The profile was used to calculate numerically the lamp motion necessary to achieve a particular surface temperature distribution.

Two basic experiments were performed; each required a different method for prescribing the lamp motion ahead of time. The first was a "spike" case, in which the lamp was rapidly moved to a specific location, left for 2.6 s, and then moved rapidly back downstream and rested over the heat sink. This motion was specified directly. The second was an "arbitrary" profile, in which the surface temperature distribution was specified. The lamp motion necessary to achieve a specified temperature distribution was found by first calibrating the lamp heat flux profile and then iteratively performing numerical simulations of the heating process until the desired surface temperature distribution was achieved. These calculations are described in detail in Hacker and Eaton (1995).

Calculating the heat flux

The primary difficulty in allowing large axial surface temperature gradients is that it becomes necessary to account for axial conduction within the substrate when computing the heat flux. Nevertheless, this correction was often minor, and for this reason, the heat flux was computed in two steps. First, the measured temperature history at each location was fitted to a one-dimensional (1-D) substrate conduction model that neglected transverse conduction. Second, a correction to account for axial conduction was estimated from the spatial second derivative of the temperature profile. The 1-D conduction model was derived assuming constant heat flux, rather than the more conventional constant heat transfer coefficient, because this is more amenable to a secondary conduction correction. For a finite-thickness plate with constant properties, insulated bottom, and suddenly imposed constant heat flux q_{1D} on the top (positive out of the surface), the analytic solution (see Carslaw and Jaeger 1959) is given by

$$T_s(t) = T_i - q_{1D} f(t)$$

$$f(t) = \frac{2\sqrt{\alpha t}}{k}\left[\text{ierfc}(0) + 2\sum_{k=0}^{\infty}\text{ierfc}\left(\frac{L_y k}{\sqrt{\alpha t}}\right)\right] \qquad (9)$$

$$\text{ierfc}(x) = \frac{1}{\sqrt{\pi}}e^{-x^2} - x\cdot\text{erfc}(x)$$

This model was fitted to the measured data $T_s(t)$ using least squares, allowing both T_i and q_{1D} to be adjusted. Next, the axial conduction was estimated as

$$\textit{Net outflow due to axial conduction} \approx -kL_y\frac{\partial^2 T}{\partial x^2} \qquad (10)$$

where k is the substrate thermal conductivity, L_y is the substrate thickness, and T is the time-averaged substrate temperature (assumed to be a function of x only). Assuming the total outflow due to both axial conduction and convection is q_{1D}, the conduction-corrected surface heat flux (q_{2D}) is found by an energy balance,

$$q_{2D} = q_{1D} + kL_y\frac{\partial^2 T}{\partial x^2} \qquad (11)$$

The second derivative was estimated from the liquid crystal measurements by fitting a second-order polynomial through a section of time-averaged surface temperature data extending ± 1 cm in both directions from the point of interest. Several additional corrections to Equation 11 were applied, in order to account for radiative losses, conduction effects at the leading and trailing edges of the test surface, and to fine-tune the estimated second derivative. These are described in detail in Hacker and Eaton (1995). However, the 1-D term generally accounted for 70–95% of the total heat transfer, except in the most highly varying cases. The Pyrex thermal properties used (see Hacker and Eaton 1992) were,

$c = 778.6 \pm 1\%$ J/kg-K

$k = 1.130 \pm 1.8\%$ W/m-K

$\rho = 2230 \pm 0.2\%$ kg/m^3

$\alpha = 6.510 \times 10^{-7} \pm 2\%$ m^2/s

Superposition technique

The experimental technique described in the Experimental apparatus and technique section is capable of measuring the heat transfer for a particular wall temperature distribution, but it does not address the general problem of predicting the heat transfer for an arbitrary wall temperature distribution without directly measuring it. The general solution can be addressed by using the linearity of the energy equation and superposition as discussed in the Existing techniques section. The nonisothermal transient technique is used to measure the data required to establish the superposition functions.

Analytical development

Mathematically, the general solution for a 2-D separated flow can be described in the same manner as the classic superposition solution (Equation 7), by allowing the unheated starting length solution to vary arbitrarily in the axial direction. For a smooth, continuously varying temperature distribution (with no discrete steps in wall temperature) the heat flux may be written:

$$q(x) = \int_{\xi=0}^{\xi=x} h(\xi, x)\frac{dT}{d\xi}(\xi)\,d\xi \qquad (12)$$

Normally the assumption of self-similarity is invoked here, to reduce the unheated starting length solution to the form $h(\xi - x)$, a function of only one variable. However, when similarity cannot

be invoked, such as in a separated flow, the unheated starting length solution remains of the form $h(\xi, x)$, and is virtually impossible to measure.

Our approach is to adapt the Anderson and Moffat (1992a, b) method for use in separated flow. We define a Green's function $g(\xi, x)$, which is the axial heat flux distribution that results when a unit impulse (Dirac delta function) of temperature difference is located at ξ. This may be written symbolically as,

$$\Delta T(x) = \delta(x - \xi) \rightarrow q(x) = g(\xi, x) \tag{13}$$

From linearity, the general heat transfer for this case is predicted by:

$$q(x) = \int_{\xi=0}^{\xi=x} g(\xi, x)\, \Delta T(\xi)\, d\xi \tag{14}$$

Now compare Equation 14 with an inverted, 1-D version of the Anderson and Moffat method-applied to a geometry composed of discrete elements,

$$q_i = \sum_j G_{ij}\, \Delta T_j \tag{15}$$

Here i and j both range from 1 to N. The discrete version is particularly interesting because it *is* so easily inverted (in two dimensions),

$$\Delta T_i = \sum_j G_{ij}^{-1} q_j \tag{16}$$

In all of these cases, it is appropriate to think of the kernel function g or G as a Green's function. Alternate versions of these equations may be developed for situations in which the temperature varies in more dimensions or in which heat can be restricted to flow only in particular directions.

The approach taken in this work was to use Equation 15 directly, by conceptually dividing the surface into 30 equal divisions in the axial direction, each of equal width (1 cm). The solution G_{ij} obtained is an approximation to the true solution represented by Equation 14. This discretization was necessitated by experimental limitations and the requirement that no restriction on the streamwise behavior of the Green's function be imposed. Continuous measurements were made with both thermocouples and liquid crystals using the nonisothermal technique. When it was necessary to discretize the continuous measurements for use in Equations 15 and 16, the liquid crystal values were averaged over each "discrete" interval.

Experimental measurement of the Green's function

In a true discrete component geometry, the Green's function G_{ij} may be measured directly. This is not possible using our transient technique, because the square spikes implied by G_{ij} cannot be physically realized on a continuous surface. It would have been possible to construct a segmented surface with individual heaters, but the practical problems of construction present a formidable challenge. Instead, the solution was accomplished by imposing and measuring heat transfer results for 30 different "spike" temperature cases that came as close as physically possible to realizing the ideal heated element and then solving a set of simultaneous equations for the common Green's function. Consider experiment 1, in which the temperature distribution ΔT_{j1} is imposed, the heat transfer q_{i1} is measured, and G_{ij} is unknown,

$$q_{i1} = G_{ij}\, \Delta T_{j1} \tag{17}$$

There are N^2 unknown elements in G_{ij} and only N equations constraining the unknowns. Next, we measure the heat transfer for $M - 1$ additional temperature distributions, to give a larger set of equations, all of which contain the same unknown Green's function:

$$q_{im} = G_{ij}\, \Delta T_{jm} \tag{18}$$

Here m (ranging from 1 to M) denotes the experiment number and i and j (ranging from 1 to N) the spatial distribution of the measurements, ΔT and q. If $M = N$, there are exactly N^2 equations, which fully constrain the Green's function. Equation 18 is actually a set of N equations of the form $A\mathbf{x} = \mathbf{b}$, and may be rearranged to make its solution more clear,

$$\begin{bmatrix} \Delta T_{11} & \cdots & \Delta T_{N1} \\ & & \\ \Delta T_{1M} & \cdots & \Delta T_{NM} \end{bmatrix} \begin{bmatrix} G_{i1} \\ \\ G_{iN} \end{bmatrix} = \begin{bmatrix} q_{i1} \\ \\ q_{iM} \end{bmatrix} \tag{19}$$

This is solved N times, yielding one row of G_{ij} each time, for $i = 1$ to N. If $M > N$, the system is overdetermined, and G_{ij} may be solved for in a least-squares sense.

Two questions arise when applying this superposition method to real measurements. First, is it possible to replace a continuous, smoothly varying temperature distribution with its pseudo-discrete version without changing the behavior of the system? It would appear that it is, because (1) as Δx approaches zero, the two must converge, and (2) our measurements verify that it works. Second, is it obvious that equally spaced "spike" temperature distributions are the best kernels to impose for each of the M experiments? This is not as clear and was not verified. However, it seemed reasonable to suppose that this approach would yield the best-conditioned experimental data.

Experimental verification

The experimental techniques for measuring the Green's function were tested in a flat-plate boundary layer where the results could be compared to simple and accurate calculations using Stan7, a 2-D boundary-layer code developed by W. M. Kays. Stan7 uses a mixing length model to compute the fluid boundary layer, and an experimental correlation for the eddy-conductivity in terms of the turbulent Prandtl number and turbulent Peclet number to compute the scalar transport (see Kays and Crawford 1993). It has been well verified in flat-plate flows against known heat transfer solutions for step and nonuniform temperature distributions, where the heat transfer was computed using the methods of the Introduction section.

Figure 4 shows results for a spike temperature case for the flat-plate boundary layer, in which the spike is located at $x = 14.7$ cm. The top part of the figure shows the temperature distribution measured by both thermocouples and liquid crystals. The bottom part shows a variety of heat transfer measurements and predictions. The solid line shows the measurement using the liquid crystal temperatures, and the dashed line shows the heat transfer computed using Stan7. Two Green's functions were computed from these data and 29 similar cases. The experimental Green's function was computed by discretizing the TLC temperature distributions to get ΔT_{jm}, and discretizing the TLC heat transfer distributions to get q_{im}, then solving Equation 19 for G_{ij}. The Stan7 Green's function was computed using the same experimental, discrete temperatures, but by discretizing the Stan7 heat transfer calculations to get q_{im}. Predictions based on both Green's functions are shown (SP stands for superposition).

Figures 5 and 6 show direct heat-flux measurements and Stan7 predictions for two specified temperature distributions for the flat-plate boundary layer. There is good agreement between the measurements and the Stan7 predictions in both cases with an rms deviation averaging 49 W/m^2. Figures 5 and 6 also include heat transfer predictions from the experimental Green's function (SP) and the Stan7 Green's function (SP-Stan7) determined from the spike cases. The rms deviation between the experimental Green's functions and the Stan7 calculations averages 43 W/m^2. Six additional specified temperature distribution cases were investigated in the flat-plate boundary layer (see Hacker and Eaton 1995). In these cases also, there was good agreement between the measurements and the Stan7 calculations (41 W/m^2 rms deviation), and the experimental superposition predictions and the Stan7 calculations (39 W/m^2 rms deviation). These measurements verified the nonisothermal transient technique and confirm the general approach of the analytical superposition technique.

A spike case for the backward-facing step is shown in Figure 7. This particular spike is located near the mean reattachment point, and the heat-flux distribution is substantially different from that of the flat-plate case (compare to Figure 4). Once again measurements were made for 30 such spike cases, and the Green's functions were evaluated. Direct measurements and superposition predictions were made for the same eight general temperature distribution cases. One example is shown in Figure 8. The rms deviation between the direct measurements and the superposition predictions is 25 W/m^2 in this figure. This is typical of the other seven cases, further substantiating the validity of the experimental superposition technique.

Detailed examination of the Green's functions

Nondimensionalization

The usual method of presenting heat transfer measurements is to define a heat transfer coefficient h based on a local temperature difference, and then to nondimensionalize h by defining a Nusselt or Stanton number. When the surface temperature varies substantially, this normalization is inappropriate, because h is ill-conditioned and ultimately undefined as the temperature difference approaches zero. However, it is clear from the definition of the Green's function that G_{ij} already accounts for the effect of changes in thermal boundary condition, and that it has the units of a heat transfer coefficient; it is, in effect, a heat transfer coefficient matrix. Therefore, it is appropriate to nondimension-

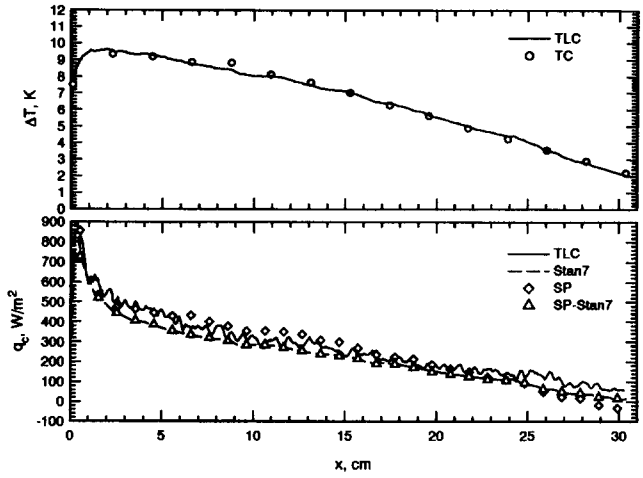

Figure 5 Flat plate boundary layer—decreasing ramp temperature profile

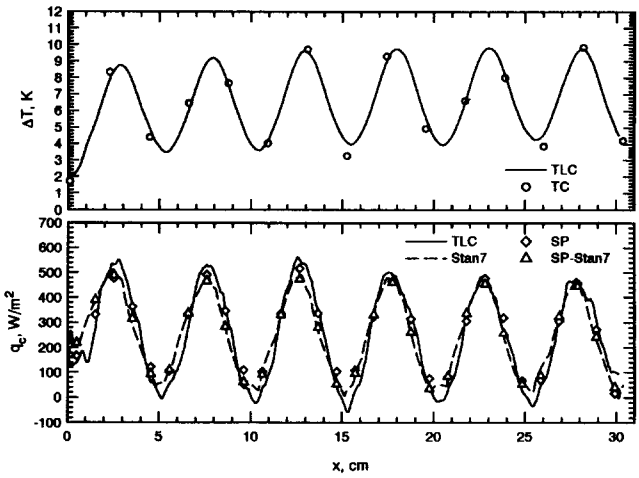

Figure 6 Flat-plate boundary layer—6-sine temperature profile

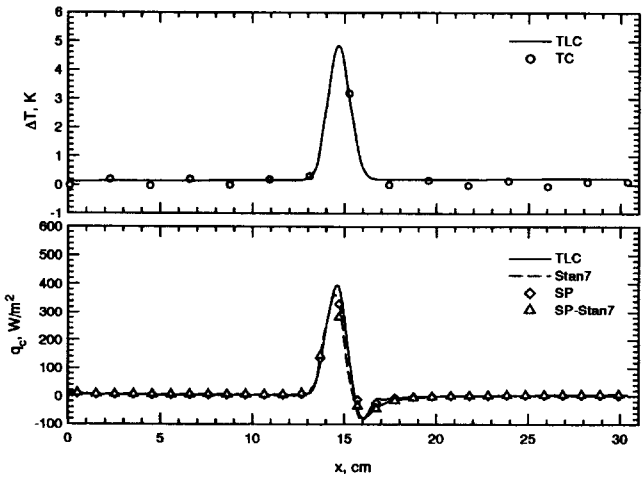

Figure 4 Flat plate—spike #15

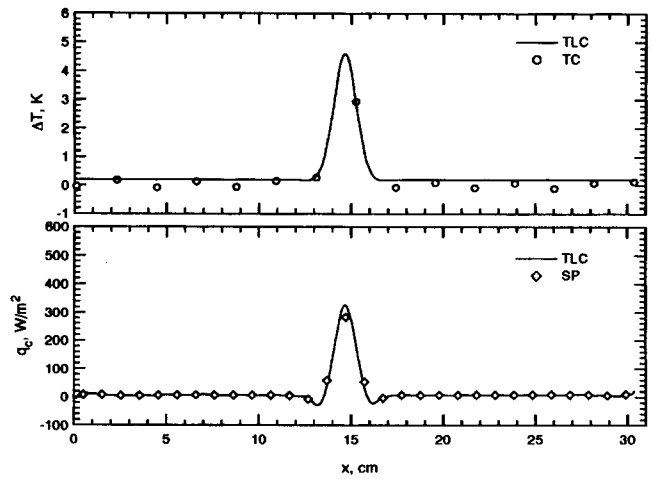

Figure 7 Backward-facing step—spike #15

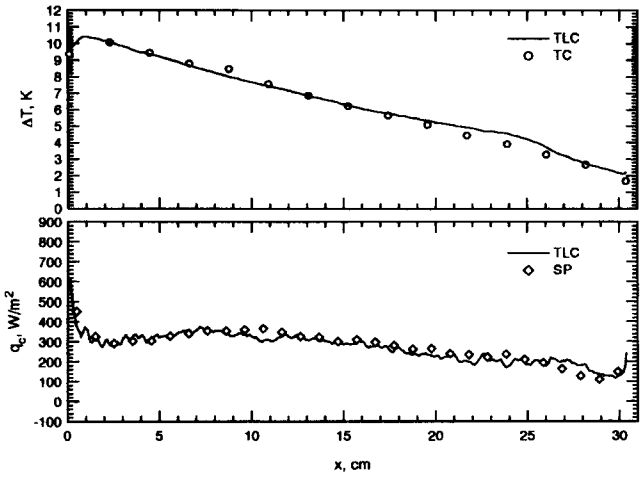

Figure 8 Backward-facing step—decreasing ramp temperature

alize the Green's function itself, forming a Nusselt or Stanton number matrix. We chose to use a Stanton number, because it is more common in separated flow studies:

$$\mathrm{St}_{ij} = \frac{G_{ij}}{\rho U_\infty C_p} \tag{20}$$

Similarly the inverse Green's function is presented nondimensionally by multiplying each entry by $\rho U_\infty C_p$.

The normalization of the streamwise coordinate is different in the two cases. In the flat-plate boundary layer, we chose the boundary-layer thickness at the start of the test plate as the appropriate scale. The streamwise coordinate is measured from the start of the test plate. In the backward-facing step, the streamwise coordinate is measured from the step and scaled by the step height. All of the Green's functions were computed by discretizing the streamwise coordinate into strips 1-cm long in the streamwise direction. The length of the strips corresponds to 0.21 boundary-layer thicknesses or 0.32 step heights.

Green's functions and inverse Green's functions

Figures 9 and 10 show one column vector ($j = 10$) from the Green's function for the flat-plate and backward-facing step flows, respectively. This is equivalent to the heat transfer distribution that would result if a 1-cm wide strip located at $x = 9.63$ cm ($j = 10$) was held at a temperature 1 K above the free-stream temperature. In the flat-plate case, the parabolic nature of the boundary layer implies that the spike response should be zero everywhere to the left of $i = 10$, positive at $i = 10$, because energy is transferred to the flow, and negative to the right (downstream), because the heated boundary layer, in turn, heats up the cooler plate. This is approximately the case, but the result is somewhat noisy and shows small negative values to the left and one positive value at $i = 12$. In the backward-facing step case, the temperature spike is located well within the recirculation region, and the response qualitatively supports this: it is negative in both directions, although somewhat more so to the left. This indicates the mean flow at this location is moving left, opposite the core flow.

A full graphical presentation of one Green's function would require 30 plots similar to Figure 9. However, note that for both cases, the Green's function is nearly zero for elements displaced by more than three increments from the temperature spike. Therefore, the entire Green's function can be presented by

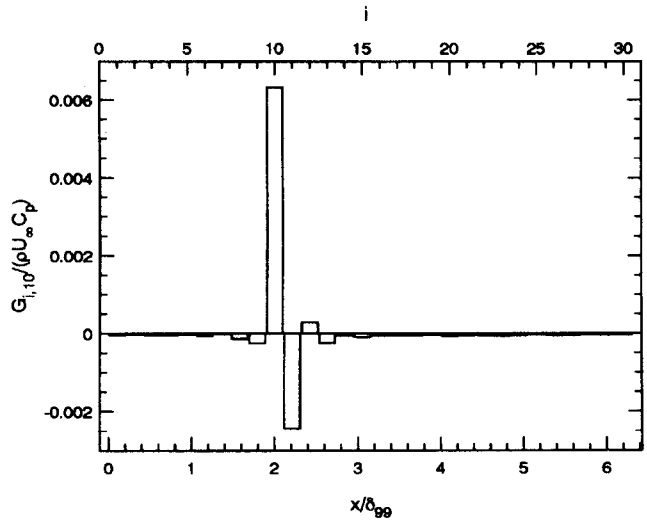

Figure 9 Flat-plate boundary layer—heat-flux distribution for temperature spike located at $j = 10$ ($x = 9.63$ cm)

plotting the components along a few diagonals of G_{ij}, as shown in Figure 11 for the flat plate and Figure 12 for the backward-facing step. This shows how the most important components of G_{ij} vary spatially. In these figures, the plotted quantity represents the value of the Green's function at position $\alpha + p$, for a spike located at α (here α is an integer). Different curves represent different diagonals, with the index p denoting the distance from the main diagonal. For example, $p = 0$ is the principal diagonal, $p = +1$ is the first component in the downstream direction, and $p = -1$ is the first component in the upstream direction. The principal diagonal is equivalent to the discrete adiabatic Stanton number of Anderson and Moffat (1992a, b).

In the flat-plate case, the boundary layer is well-developed, and the Reynolds number changes by only a few percentage points over the length of the test surface. Therefore, the Green's function is nearly constant. All components except those on the principal diagonal and $p = +1$ are very small. In the backward-facing step case, there is significant although gradual spatial variation of G_{ij} along the test surface. The principal component has a relatively low value in the recirculation region and then

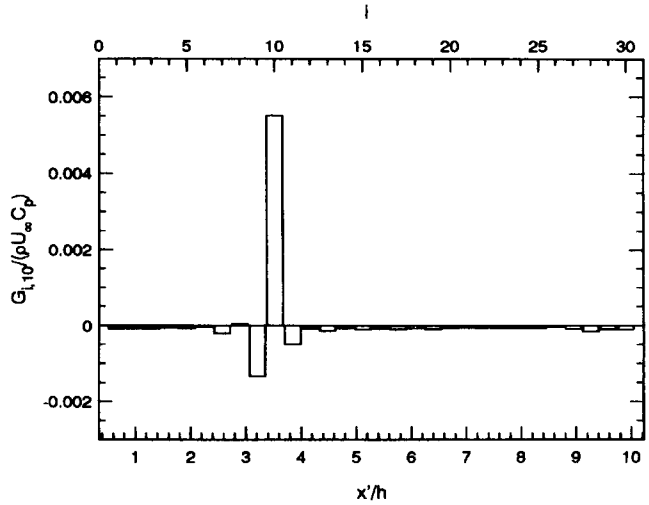

Figure 10 Backward-facing step—heat-flux distribution for temperature spike located at $j = 10$ ($x = 9.63$ cm)

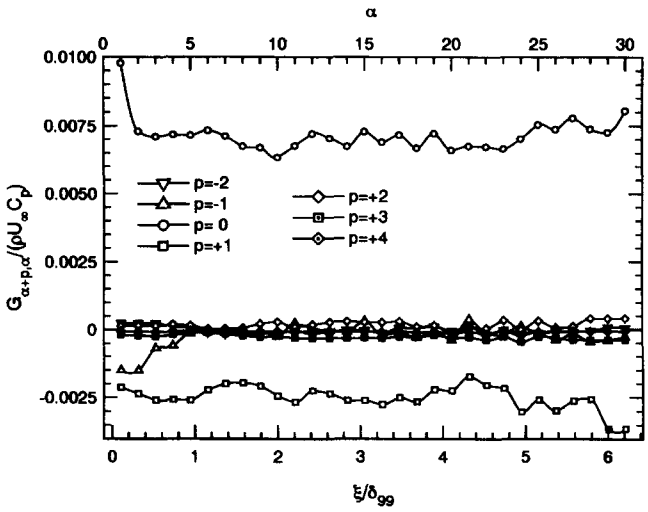

Figure 11 Flat-plate boundary layer—distribution of principal components of Green's function.

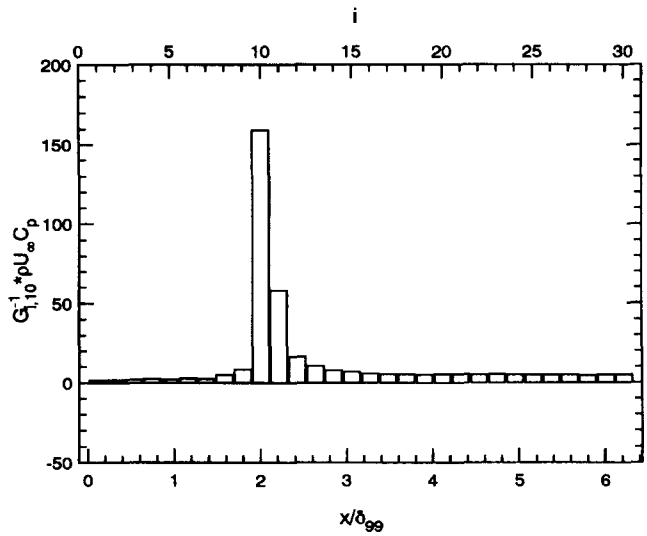

Figure 13 Flat-plate boundary layer—temperature distribution for heat flux spike located at $j=10$ ($x=9.63$ cm)

increases slowly to a higher level near the reattachment point. The behavior of the $p=+1$ and $p=-1$ components is more interesting. The upstream component ($p=-1$) is initially strongly-negative then rises toward zero. The downstream component is small in the recirculation region and becomes more negative moving downstream. The values of the two components are nearly equal at the reattachment point.

It is instructive to examine the inverse Green's function obtained by inverting the experimentally measured Green's function. One column of the inverse Green's function may be thought of as the temperature distribution that would be measured on an adiabatic wall when a 1-cm wide, 1 W/m^2 spike of heat flux is located at a specified location. Figures 13 and 14 show the column of the inverse Green's function representing heating at $x=9.63$ cm ($j=10$). In the flat plate case (Figure 13), the parabolic nature of the boundary layer implies that the response should be zero everywhere to the left of $i=10$, positive at $i=10$, because energy is transferred to the flow, and asymptotically drop to zero far downstream of the heated location. This pattern is apparent in the figure, although noise causes some spurious values upstream of heating and fluctuations in the downstream values. In the backward-facing step case (Figure 14), we would expect the resulting temperatures to drop asymptotically to zero toward the far right, but not necessarily to zero in the recirculation region to the left. This behavior is, indeed, observed. The data from the central diagonals of the inverse Green's functions can be plotted in the same way as before. However, the values do not decay as rapidly moving off of the principal diagonal. The plot for the flat-plate boundary layer shows constant values, as would be expected. Thus, the entire inverse Green's function is adequately represented by Figure 13. Figure 15 shows the values on the diagonals for the backward-facing step. The value on the $p=-1$ diagonal falls moving downstream, while the value on the $p=+1$ diagonal rises. The two values cross in the reattachment region. The same trend is seen for the $p=\pm 2$ diagonals.

Looking at the Green's functions for both flows, it is striking that the response to a 1-cm wide temperature spike is confined to a relatively small spatial region: about 95% of the total heat transfer appears to be within ± 1.5 cm of the spike location. In contrast, the inverse Green's functions show that the tempera-

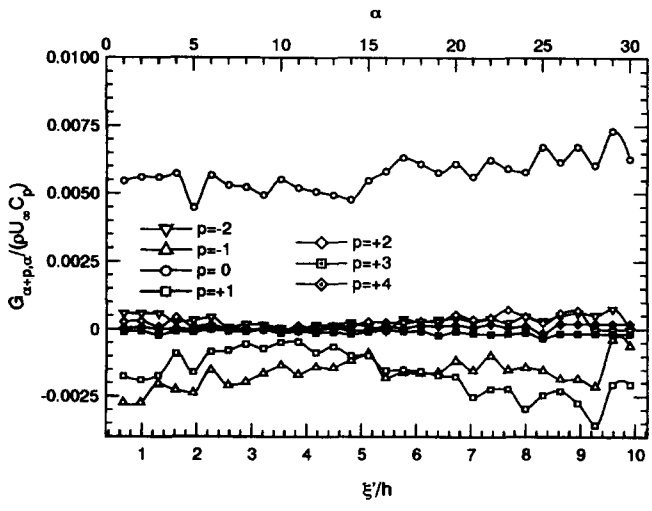

Figure 12 Backward-facing step—distribution of principal components of Green's function

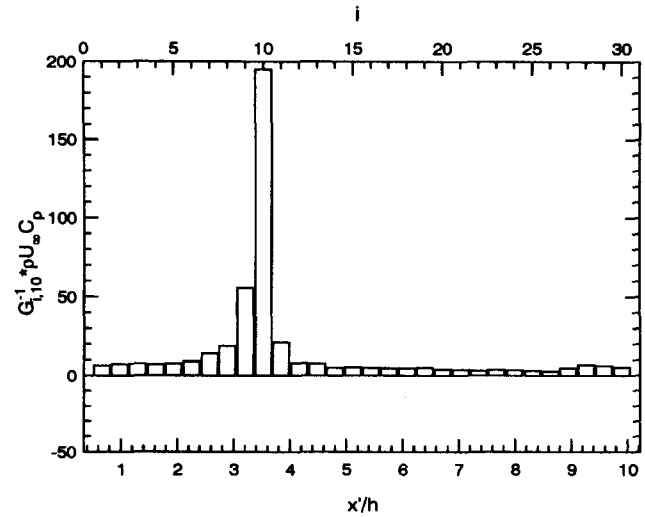

Figure 14 Backward-facing step—temperature distribution for heat flux spike located at $j=10$ ($x=9.63$ cm)

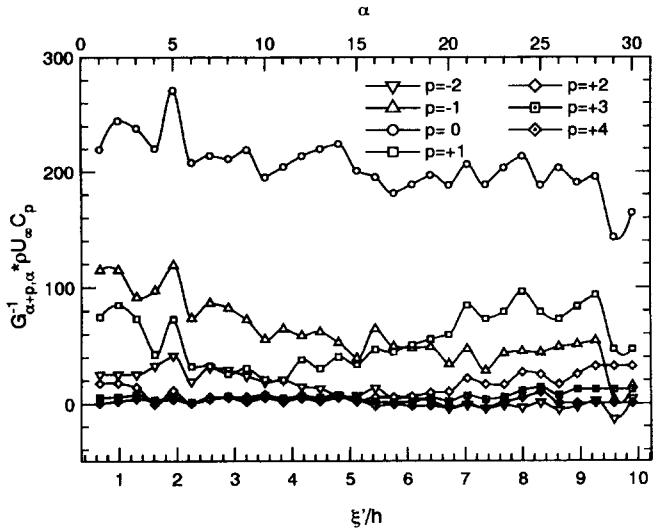

Figure 15 Backward-facing step—distribution of principal components of inverse Green's function

ture effect of a 1-cm wide heat flux spike is considerably more spread out. In the flat-plate case, the temperature effect carries approximately 4–5 cm (1 boundary-layer thickness) downstream. In the backward-facing step case, the effect carries out to about ±3 cm (one step height). In contrast, the inverse Green's function is 2–3 times more diffuse in both cases.

General discussion

We have shown that the nonisothermal transient technique is capable of providing accurate measurements of the heat transfer given a prescribed surface temperature distribution. We have also shown that the new superposition technique based on experimentally determined Green's functions can accurately predict the effect of arbitrary temperature boundary conditions. This technique is applicable to both attached boundary-layer flows and more complicated separated flows where the hydrodynamics are not self-similar, and flow reversal occurs. However, the technique is difficult to implement for a new flow, because calculation of the Green's functions requires conducting a large number of independent experiments (30 in the case illustrated above) and solving a set of coupled equations to get the Green's functions. The set of equations is somewhat ill-conditioned, and it would probably be impossible to solve a significantly larger set of equations given the accuracy of the available heat flux measurements.

There are a number of improvements that could make measurements of the effect of thermal boundary conditions much more practical. First, it would appear that direct measurement of the inverse Green's function (instead of the Green's function) would be numerically better conditioned, because of its more "diffuse" nature. This cannot be done using the current nonisothermal transient technique, but could be accomplished using a movable constant heat flux point or line source embedded in an adiabatic surface, in conjunction with high-resolution surface temperature measurements. This approach would allow steady-state measurements and avoid the necessity of solving a large set of simultaneous equations involving 30 or more separate experiments. In addition, two requirements restricting the form of the solution could theoretically be introduced to precondition the result. First, by the 2nd law of Thermodynamics, each of the elements of the inverse Green's function must be positive. Second, the highly banded nature of the solution could be imposed *a priori* to restrict the solution and effectively improve the resolution of the measurements.

The question remains as to the generality of the separated flow results presented here. Strictly speaking, the Green's functions are applicable only to the precise flow geometry and Reynolds number found in this experiment. To obtain predictions for a new case, one would require a new Green's function measured in that flow. However, the present results show that the Green's function is really quite simple in the separated and reattaching flow. An impulse of temperature on the wall affects only a small region on either side of the impulse. For the backward-facing step, the Green's function decayed to a negligible value within a distance of about 0.5 step heights or less than 1/10 of the reattachment length. The value of the Green's function on the central diagonal changed slowly, increasing as it approached the reattachment point. The value of the two components on either side of the principal diagonal varied in a logical way: the upstream component was large in the recirculating region and slowly decayed downstream, while the downstream component was small in the recirculating region and slowly increased moving downstream. The two off-diagonal components had approximately equal values at reattachment.

If we knew how to scale the components of the Green's function, we could then use the information above to predict the heat transfer distribution in any separated and reattaching flow. Scaling of the streamwise coordinate by the reattachment length has been well established by previous workers. Scaling of the heat transfer rate is not quite as well established. Vogel and Eaton (1984) showed that the Stanton number distribution for contact heat flux boundary conditions collapsed well when normalized by the peak value which occurred near reattachment. Baughn et al. (1984) found that the maximum heat transfer rate scaled as $Re^{2/3}$ in the pipe expansion. Therefore, it may be possible, to estimate the heat transfer rate in a separated flow with an arbitrary wall temperature distribution by measuring only the heat transfer rate from a heated spot at the reattachment point at a single Reynolds number. This conclusion must be treated as speculation until further data are acquired for other geometries and Reynolds numbers.

Acknowledgments

Preliminary support for this project was supplied by the National Science Foundation under grant CTS 90-14814. We also thank Professor Robert Moffat for use of his liquid-crystal temperature measurement system.

References

Adams, E. W. and Johnston, J. P. 1988. Flow structure in the near-wall zone of a turbulent separated flow. *AIAA J.*, **21**, 932–935

Amano, R. S., Jensen, M. K. and Goel, P. 1983. A numerical and experimental investigation of turbulent heat transport downstream from an abrupt pipe expansion. *J. Heat Transfer*, **105**, 862–869

Anderson, A. M. and Moffat, R. J. 1992a. The adiabatic heat transfer coefficient and the superposition kernel function: Part 1—Data for arrays of flatpacks for different flow conditions. *J. Electronics Packaging*, **114**, 14–21

Anderson, A. M. and Moffat, R. J. 1992b. The adiabatic heat transfer coefficient and the superposition kernel function: Part 2—Modeling flatpack data as a function of channel turbulence. *J. Electronics Packaging*, **114**, 22–28

Aung, W. 1982. Separated forced convection, *Proc. ASME-JSME Thermal Engineering Joint Conference*, vol. 2, ASME NY, 499–515

Aung, W. and Watkins, C. B. 1979. Heat transfer mechanisms in separated forced convection. In *Turbulent Forced Convection in Channels and Bundles*, S. Kakac and D. B. Spaulding, (eds.), vol 1, 233–257 Hemisphere, Washington

Baughn, J. W., Hoffman, M. A., Lauder, B. E. and Takahashi, R. K. 1984. Local heat transfer downstream of an abrupt expansion in a circular channel with constant wall heat flux. *J. Heat Transfer*, **106**, 789–796

Baughn, J. W., Hoffman, M. A., Launder, B. E., Lee, D. and Yap, C. 1989. Heat transfer, temperature, and velocity measurements downstream of an abrupt expansion in a circular tube at uniform wall temperature. *J. Heat Transfer*, **111**, 870–876

Carslaw, H. S. and Jaeger, J. C. 1959. *Conduction of Heat in Solids*, 2nd ed. Clarendon Press, Oxford

Chyu, M. K. and Goldstein, R. J. 1986. Local mass transfer in rectangular cavities with separated turbulent flow. *Heat Transfer, Proc. 8th Intl. Heat Transfer Conf.*, vol. 3, Hemisphere, Washington 1065–1070

Farina, D. J. and Moffat, R. J. 1994. A system for making temperature measurements using thermochromic liquid crystals. Dept. of Mechanical Engineering, Stanford University, Stanford, CA, Report No. HMT-48

Garcia, A. and Sparrow, E. M. 1987. Turbulent heat transfer downstream of a contraction-related, forward-facing step in a duct. *J. Heat Transfer*, **109**, 621–626

Hacker, J. M. and Eaton, J. K. 1992. A heat transfer measurement technique which allows arbitrary wall temperature distributions. *Proc. 28 National Heat Transfer Conference*, San Diego, CA

Hacker, J. M. and Eaton, J. K. 1995. Heat transfer measurements in a backward-facing step flow with arbitrary wall temperature variations. Dept. of Mechanical Engineering, Stanford University, Stanford, CA, Report. No. MD-71

Kays, W. M. and Crawford, M. E. 1993. *Convective Heat and Mass Transfer*, (3rd ed.). McGraw-Hill

Mori, Y., Uchida, Y. and Sakai, K. 1986. A study of the time and spatial structure of heat transfer performance near the reattaching point of separated flows. *Proc. Intl. Heat Transfer Conf.*, vol. 3, Hemisphere, Washington 1083–1088

Orlov, V. V., Ovchinnikov, V. V., Mukhina, N. N. and Karsten, V. M. 1984 Investigation of turbulence and heat transfer in a separating flow behind a step. *Heat Transfer—Soviet Res.*, **16**

Ota, T. and Nishiyama, H. 1987. A correlations of maximum turbulent heat transfer coefficient in reattachment flow region. *Int. J. Heat Mass Transfer*. **30**, 1193–1200

Schultz, D. L. and Jones, T. V. 1973. Heat transfer in short duration hypersonic facilities. AGARDograph No. 165

Shisov, E. V., Roganov, P. S., Grabarnik, S. I. and Zabolotsky, V. P. 1988. Heat transfer in the recirculating region formed by a backward-facing step. *Intl. J. Heat Mass Transfer*, **31**, 1557–1562

Sparrow, E. M. 1988. Heat transfer in fluid fows which do not follow the contour of boundary walls, *J. Heat Transfer*, **110**, 1145–1153

Sparrow, E. M. and Ohadi, M. M. 1987. Comparison of turbulent thermal entrance regions for pipe flows with developed velocity and velocity developing from a sharp-edged inlet. *J. Heat Transfer*, **109**, 1028–1030

Tribus, M. and Klein, J. 1952. Forced convection from non-isothermal surfaces. *Proc. Heat Transfer Symposium*, University of Michigan, Ann Arbor, MI

Vogel, J. C. and Eaton, J. K. 1984. Heat transfer and fluid mechanics measurements in the turbulent reattaching flow behind a backward-facing step. Ph.D. thesis, Thermosciences Division, Dept. of Mechanical Engineering, Stanford University, Stanford, CA, Rept. MD-44

Vogel, J. C. and Eaton, J. K. 1985. Combined heat transfer and fluid dynamics measurements downstream of a backward-facing step. *J. Heat Transfer*, **107**, 922–929

Wakisaka, N. 1986. Heat transfer in the reattachment region of a sudden expansion flow in ducts. *Heat Transfer Res.* **5**, 65–76